Solvolysis of Benzal Chloride Under Vibrational Strong Coupling

Yashika Gupta

MS16051

A dissertation submitted for the partial fulfilment of

BS-MS dual degree in Science

Department of Chemical Sciences

Indian Institute of Science Education and Research Mohali

April 2021

Certificate of Examination

This is to certify that the dissertation titled “Solvolysis of Benzal Chloride under Vibrational Strong Coupling”, submitted by Yashika Gupta (Reg.No.MS16051) for partial fulfilment of the BS-MS dual degree programme of the institute, has been examined by the thesis committee duly appointed by the institute. The committee finds the work done by the candidate satisfactory and recommends that the report be accepted.

Dr. P. Balanarayan Dr. Sugumar Venkataramani Dr. Jino George

(Supervisor)

Dated: April 30, 2021

Declaration

The work presented in this dissertation has been carried out by me under the guidance of Dr. Jino George at the Indian Institute of Science Education and Research Mohali.

This work has not been submitted in part or in full for a degree, a diploma, or a fellowship to any other university or institute. Whenever contributions of others are involved, every effort is made to indicate this clearly, with due acknowledgement of collaborative research and discussions. This thesis is a bonafide record of original work done by me, and all sources listed within have been detailed in the bibliography.

Yashika Gupta
(Candidate)

Dated: April 30, 2021

In my capacity as the supervisor of the candidate's project work, I certify that the above statements by the candidate are true to the best of my knowledge.

Dr. Jino George
(Supervisor)

Acknowledgement

I would like to express my deepest appreciation to all those who provided me with the possibility to complete my MS thesis. A special gratitude I give to Dr. Jino George, who allowed me to work under his guidance. On many occasions, he has given valuable suggestions that motivated me for learning new things in science.

I also appreciate my thesis committee members Dr. P.Balanarayan and Dr. Sugumar, to provide me with an opportunity to present my work and for their thoughtful suggestions.

Secondly, I would like to thank Mr. Jaibir, whose stimulating suggestions and encouragement helped me to coordinate my project and in writing this thesis. I have to appreciate the guidance given by all the lab members for their encouraging comments, valuable inputs and support throughout my work.

Furthermore, I would also like to acknowledge IISER Mohali for the instrumental and other infrastructural facilities.

At last, I would like to thank my parents, my brother, and my friends for the motivation to accomplish my work.

List of figures

List of Schemes

List of Tables

Notations

SC = Strong Coupling

VSC = Vibrational Strong Coupling

ε_{vac} = vacuum electric field strength

ω_c = frequency of the cavity

ε_0 = vacuum pertmitivity

V = mode volume of the cavity

$\vec{d}$ = transition dipole moment

$\widehat{H}_{JC}$ = Jaynes-Cummings Hamiltonian

$\widehat{H}_{cav}$ = Electric field Hamiltonian

$\widehat{H}_{mol}$ = Molecular Hamiltonian

$\widehat{H}_{int}$ = Hamiltonian for molecule-field interaction

P^+ = Upper Polaritonic State

P^- = Lower Polaritonic State

$\hbar\Omega_R$ = Rabi splitting

n_{ph} = number of photons

cQED = cavity quantum electrodynamics

$k_{||}$ = in-plane momentum

Q = Quality factor

FSR = free spectral range

FTIR = Fourier Transform Infrared Spectroscopy

ACN = Acetonitrile

λ_{max} = Maximum absorbance wavelength

OD = optical density

A = Absorbance

c = concentration

l = path length

ε = molar extinction coefficient

Contents

Abstract

Over the last few years, theoretical and experimental studies observed that the moulding of the chemical reaction landscape had been made possible by selective vibrational strong coupling (VSC) of the reactant molecules. In VSC, the excited vibrational state undergoes strong coupling with the photon in an infrared cavity, leading to the formation of new vibro-polaritonic states. In the current project, our motive is to study the effects of VSC on controlling the reaction rate. For this purpose, we chose the solvolysis reaction of benzal chloride with water, leading to the formation of benzaldehyde as the final product. This reaction follows an S_N1 mechanism in which the cleavage of the C-Cl bond is the rate-determining step. So we tried to couple C-Cl stretch frequency inside an optical cavity. Due to poor oscillator strength and lower concentration of C-Cl, we barely managed to get direct coupling in the system, whereas the rate control was little due to weak interactions. As a next step, we also tried the coupling of the O-H stretching mode of water molecules, which can trigger the reaction rate control by co-operative interaction or by directly involving in the solvolysis process. In this thesis, we optimized the conditions for kinetic experiments in both non-cavity and cavity conditions and further suggested the option of doing the experiments in base-catalyzed and buffer mediated conditions. Further studies are required to completely understand the effect of VSC on these classes of molecular reactions.

Chapter 1: Introduction

1.1 Historical Background

All the matter that surrounds us is made up of a combination of atoms. Atoms are held together by different attractive forces and chemical bonds in different chemical species. The fundamentals of physical and chemical sciences are based on the fact that intrinsic properties of matter or molecules can be altered as they are associated with atoms. Moreover, this is independent of their environment. Besides, current material science is created around the premise that the critical condition for tuning physical properties and chemical reactivity is moulding the chemical bonds and intermolecular interactions.[1]

Exciton coupling is one of the examples which show how intermolecular interaction can change molecular properties. The factors that affect the strength of exciton-exciton coupling are the magnitude of transition dipole moment, the relative orientation between monomers, and intermolecular distance. Coulomb interactions between the transition dipole moments of different molecules would be significant if the distance between molecules is small enough. This results in the resonant energy transfer within the aggregate from a donor molecule to an acceptor, i.e., excitation is delocalised. The system is characterised based on the relative orientation of transition dipole moments by absorption spectra of aggregates: J-aggregates (redshifted) and H-aggregates (blue shifted), shown in figure 1.1.[2,3]

Very recently, strong coupling comes into play. Studies have been reported that strong coupling can affect several phenomena at molecular levels, such as phase transitions, chemical reactions, and conductivity.[4] Before the 20th century, light and matter were

regarded as separate entities with their peculiar properties. After the experimental demonstration of the Purcell effect[5] and exciton-surface plasmon strong coupling of Langmuir Blodgett films on a silver surface, this field starts expanding [6].

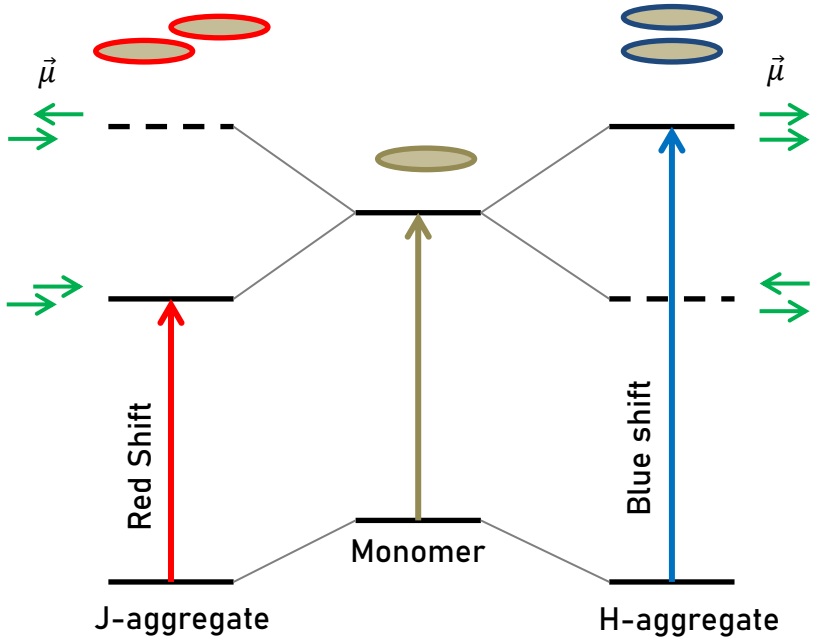

Figure 1.1: Schematic energy diagram of H- and J-aggregates formed by electronic coupling between transition dipole moment and new energy levels are forming.

1.2 Light-Matter Strong Coupling

1.2.1 Theoretical Background

Strong coupling can be regarded as the interaction of light and matter states in optical cavity configuration and forming new hybrid states overcoming all dissipative processes. The light-matter strong coupling can be understood by the classical analogy of coupled harmonic oscillator. Two harmonic oscillators behave independently when they are not coupled, and they both have their own frequency. However, when they are coupled strongly, both oscillators behave as a single entity by exchanging their energy periodically. This

phenomenon will lead to the formation of two new energy modes having different frequencies, and separation between these modes is known as Normal mode splitting. (figure 1.2) [7]

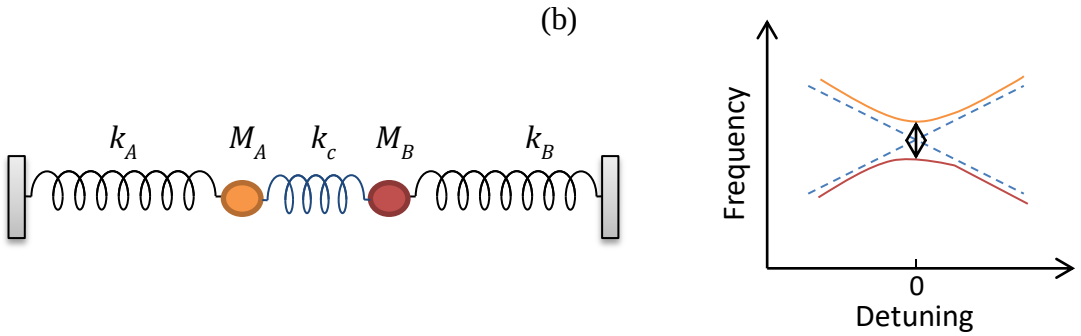

Figure 1.2: Schematic diagram of a) two classical harmonic oscillator coupled together, b) showing anticrossing behaviour, where two new normal modes are forming ω_+ and ω_- separated by 2Ω (normal mode splitting energy).

A large number of experimental results of strong coupling are feasible to explain by classical description. However, it is inadequate to explain all the aspects of Strong coupling like entanglement due to the presence of vacuum fluctuations. Vacuum fluctuations are defined as "ground state energy of the quantised electromagnetic field." The vacuum field can be directly measured, and the strength of the vacuum field in the optical cavity is given by the following equation-

$$\varepsilon_{vac} = \sqrt{\frac{\hbar\omega_c}{2\varepsilon_0 \upsilon}}$$

Where, ε_{vac} is vacuum electric field strength, ω_c is the resonance frequency of the cavity, ε_0 is vacuum permittivity, and υ is mode volume of the cavity. [7, 8]

1.2.2 Quantum description of strong coupling

Strong coupling of light-matter as the coupled quantised harmonic oscillator is based on several approximations.

For light-matter interaction, the most crucial parameter is the transition dipole moment. The transition dipole moment is similar to other dipole moments. It causes the transition of an electron from the ground state (ψ_i) to an excited state (ψ_f). The following expression gives strength of transition dipole moment ($\vec{d}$)-

$$\vec{d}_{i\to f} = \langle \psi_f | \hat{d} | \psi_i \rangle$$

The light-matter coupling is given by:

$$\vartheta = -\vec{d}.\vec{\varepsilon}$$

Here, ϑ is the strength of coupling between light and matter and $\vec{\varepsilon}$ is the electric field operator. [9, 10] Based on the strength of interaction, Light-matter can be classified into three regimes: Weak Coupling, Strong Coupling, and Ultra Strong Coupling.

1.2.3 Weak coupling regime

Typically, the coupling is weak between electromagnetic field and matter. Due to which it is possible to consider both of them as separate entities which can exchange energy. These exchanges are calculated using Fermi's Golden Rule, which states that in coupled electromagnetic modes, the density of states affects the spontaneous emission rate. As a result, the spontaneous emission rate can be increased or decreased by changing the density of states known as the Purcell effect.[11]

When a molecule inside a cavity is in resonance with the field mode, there is an enhancement in the spontaneous rate of emission due to an increase of photon density of states inside the cavity as compared to the free space density of states.[7]

1.2.4 Strong coupling regime

Inside the resonant cavity, when a molecule absorbs the photon and then emits, the photon is reflected by the mirrors back and forth, and subsequently, it remains inside the cavity. So, the reabsorption chances of the photon by the molecule are increased. Considering the probability of reabsorption is higher than the rate of non-resonant decay of the molecule and leakage of a photon from the mirror. In that case, the system is in a strong coupling regime.

1.2.5 Properties of strong coupling regime

Strong coupling can be understood by cavity quantum electrodynamics (cQED). It depicts the properties of the coupled atomic system with the quantised electromagnetic field. This system is best described by Jaynes-Cummings Hamiltonian ($\widehat{H}_{JC}$) which describes the system as a sum of electric field ($\widehat{H}_{cav}$), molecule ($\widehat{H}_{mol}$) and molecule-field interaction ($\widehat{H}_{int}$) and is given by:

$$\widehat{H}_{JC} = \widehat{H}_{mol} + \widehat{H}_{cav} + \widehat{H}_{int}$$

In a strong coupling regime, the interaction of light and matter states in the optical cavity forms new hybrid states. The newly formed dressed states of the molecule-field system are known as polaritonic states ($|P^+\rangle$ and $|P^-\rangle$). The wavefunctions of these two eigenstates obtained by diagonalising Jaynes-Cummings Hamiltonian are:

$$|P^+\rangle = \alpha|e,0\rangle + \beta|g,1\rangle$$

$$|P^-\rangle = \beta|e,0\rangle - \alpha|g,1\rangle$$

where, $|0\rangle$ and $|1\rangle$ are photonic states of the cavity, g is the ground state of the molecule, e is excited state of molecule and α and β are Hopfield coefficients.[12,13] These hybrid light-matter states form only when resonant energy exchange between cavity and molecule is faster than any dissipative process. The separation between these hybrid states is known as Rabi splitting, as shown in figure 1.3. Rabi splitting is given by-

$$\Delta E = E_+ - E_- = \hbar\Omega_R = 2V_n = 2d.E_0 = 2d\sqrt{\frac{\hbar\omega}{2\varepsilon_0 \upsilon}} \times \sqrt{n+1}$$

Here, V_n is the interaction energy between the electric component of an electromagnetic field, E_0 and transition dipole moment of material (d), $\hbar\omega$ is the resonant energy, ε_0 is the vacuum permittivity, υ is the volume of the electromagnetic mode, and n is the number of photons involved in the coupling process.

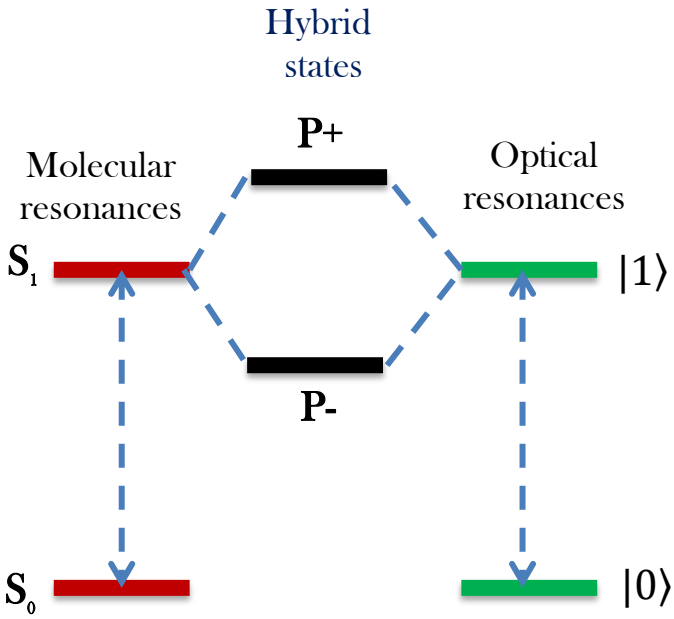

Figure 1.3: Schematic diagram of coupling between molecular transition dipole moment with cavity resonance (optical mode), forming new Light-matter hybrid polaritonic states $|P^+\rangle$ and $|P^-\rangle$ and splitting between them is $\hbar\Omega_R$.

In the absence of dissipation, the Rabi splitting becomes:

$$\hbar\Omega_R = 2V_n = 2d\sqrt{\frac{\hbar\omega}{2\varepsilon_0 \upsilon}} \times \sqrt{n_{ph+1}}$$

Here, $\hbar\omega$ is the resonant energy, ε_0 is the vacuum permittivity, υ is the volume of the electromagnetic mode, and n_{ph} is the number of photons involved in the coupling process.

When $n_{ph} = 0$, that is, in the absence of photons, there will be some splitting energy referred to as vacuum Rabi splitting. It suggests that strong coupling is possible at zero-point energy via vacuum fluctuations. Vacuum fluctuations are finite zero-point energy of quantised electromagnetic field confined inside a cavity. The magnitude of Rabi splitting reflects the strength of the interaction. Rabi splitting is directly proportional to the square root of the concentration of molecules, so as the concentration increases, Rabi splitting also increases.[4]

At resonance, the strength of coupling is controlled by the rate of decay of photon in the cavity (κ), rate of decay of molecule (γ), and coupling strength (g). When $g \ll (\kappa, \gamma)$, the system is said to be in the weak coupling regime but if $g \gg (\kappa, \gamma)$, then the system will be in the strong coupling regime. Furthermore, as previously discussed, in a strong coupling regime, coupling interaction is faster than any dissipative process. Experimentally κ and γ are related to cavity linewidth and molecular absorption band line width. To ensure if the system is in strong coupling in the experiment, one should check whether the splitting (Ω_R) is larger than the full-width half-maxima (FWHM) of the molecular absorption band ($\Delta\omega_x$) and the cavity mode ($\Delta\omega_c$).[14, 15]

$$\Omega_R > \frac{\Delta\omega_x + \Delta\omega_c}{2}$$

The relative coupling strength is measured using the ratio between the frequency of the cavity mode and the Rabi frequency. The system will be in the ultra-strong coupling regime, if this ratio is greater than 0.1 to 0.2. In this regime, the coupling energy is significant in comparison with molecular transition energy.[16]

1.2.6 Properties of Hybrid polaritonic states

I. Collective states

As already mentioned, Rabi splitting energy enhances significantly on increasing concentration of molecules strongly coupled in an optical cavity with resonance mode. Other molecular eigenstates levels (not involved directly in coupling) are also perturbed

due to this large splitting, as shown in figure 1.4. This means N+1 collective states are generated by N molecules. From these N+1 states, only two states ($|P^+\rangle$ and $|P^-\rangle$) are detectable, and as the transition in other N-1 states are forbidden from the ground state, so these states are called collective dark states, illustrated in figure 1.4.[17]

So basically, polaritons show collective behaviour, i.e., a large no of molecules can get couple in a single optical mode at a time. When a molecule interacts with the cavity, it emits the photon, which will be absorbed by another molecule. This phenomenon happens several times before the cavity photon is lost.

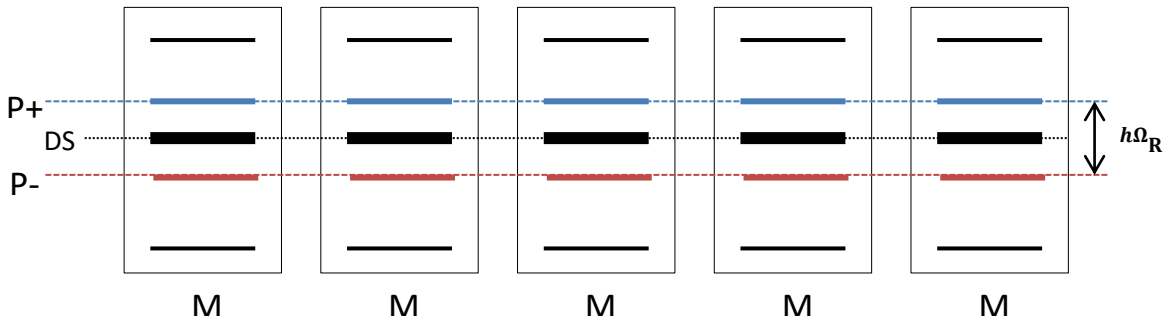

Figure 1.4: Illustration of collective behaviour of polaritons, collective states of polaritons (P_+, P_- and Dark state (DS)) delocalised over many molecules.

II. Angular Dispersion

Polaritonic states are hybrid states of light and matter, so they inherit their behaviour from both light and matter. Polaritonic states show dispersive behaviour due to the photonic component that is, they show dependence on momentum and angle. To study this dependence, a graph between energy and in-plane momentum $k_{||}$ is plotted (figure 1.5). In-plane momentum dependence on an angle is the following;

$$|k_{||}| = \frac{2\pi}{\lambda} sin\theta$$

Here, λ is the wavelength of the peak and θ is the incidence angle. The intersection of dispersive optical component and non-dispersive absorption band of the molecule leads

to an anticrossing. At Rabi splitting, material and photonic components are isoenergetic, and they have equal contribution in hybrid polaritonic states. As $k_{||}$ increases, the contribution of the photonic part shifts from $|P^-\rangle$ to $|P^+\rangle$. [18]

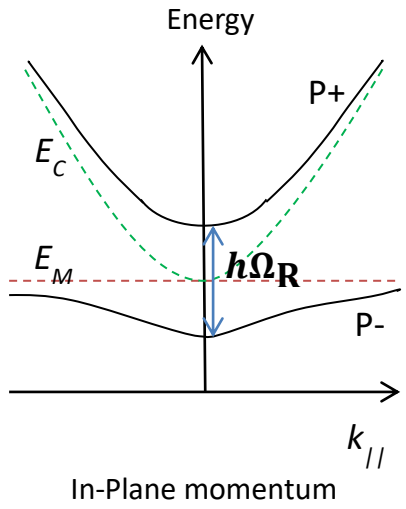

Figure 1.5: Illustration of dispersive behaviour of polaritonic states in an FP cavity which is tuned in such a way that the anticrossing appears at normal incidence ($k_{//} = 0$) i.e., absorber is in resonance with optical mode at normal incidence. Here, E_C is the FP cavity resonance and E_M is the molecular transition energy.

1.2.7 Optical Cavity

Experimentally light-matter strong coupling is done in Fabry-Perot (FP) cavity, shown in figure 1.6. FP cavity is an optical cavity in which mirrors are arranged in such a way that they work as standing wave resonator for electromagnetic waves.[19] The cavity contains two BaF_2 windows that are coated with a thin gold layer on top. Then both the mirrors are placed parallel to each other with a spacer in between them. Light can bounce back and forth between the mirrors and form a standing wave pattern.

When the cavity is in on- resonance condition, then the length of the cavity (L_{cav}) is an integral multiple of intra-cavity half wavelengths:

$$L_{cav} = m\left(\frac{\lambda}{2n}\right)$$

Here, λ is the wavelength of light, and n is the refractive index of the medium. The dissipation of energy from the cavity is characterised by the Quality factor (Q):

$$Q = \frac{\omega_R}{\Delta\omega_C}$$

where, ω_R is the resonant frequency and $\Delta\omega_C$ is FWHM of the cavity mode. The more the Q-factor, the lesser will be the energy dissipation from the cavity. By increasing the reflectivity of the mirrors, a high Q-factor can be achieved.[7]

For studying the strong coupling, mirrors are usually made of IR transparent substrates like ZnSe, BaF_2, and CaF_2.

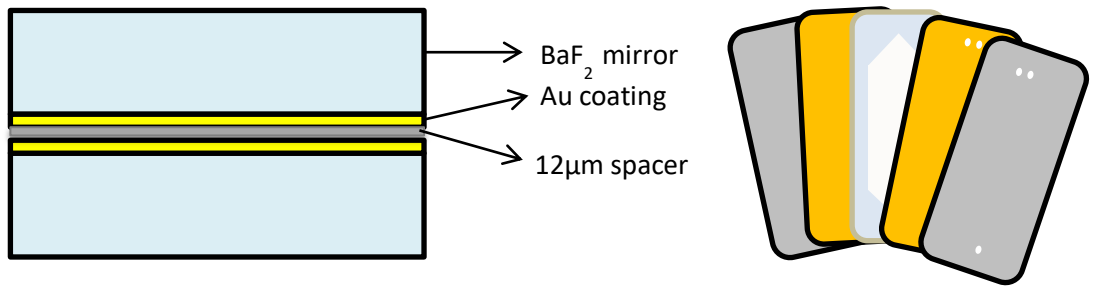

Figure 1.6: Schematic diagram of a Fabry-Perot Cavity with barium fluoride substrates, coated with gold mirrors separated by Mylar spacer of 12µm.

In IR spectra of FP cavity, uniformly separated cavity modes are formed. Based on the spacer thickness, one can vary the position of the optical modes of the cavity. The energy difference between optical modes is known as Free spectral range and calculated by the following formula:-

$$FSR = \frac{10000}{2nl}$$

Here, n= refractive index and l is the length of the cavity in microns explicitly.

1.2.8 Vibrational Strong Coupling (VSC)

Strong coupling is not limited to only electronic transition, but it is also possible in vibrational transitions. However, the effect of coupling is different because vibrational transitions are of lower energy than electronic transitions. When cavity mode is coupled to vibrational transition, vibrational level splits into Vibro-polaritonic states and the energy gap between $|P^+\rangle$ and $|P^-\rangle$ is vibrational Rabi splitting. Modification of bond lengths and potential surfaces of bond association and dissociation is possible by changing the strength of the oscillator of molecular vibration. It is also possible to alter the rate of a chemical reaction by strongly couple vibration mode in the optical cavity. Even in the absence of light, rates can be modified, which makes it different from catalysis.[20]

Many studies have been conducted on chemical reactions in recent years to see the change in chemical reactivity under the influence of VSC. But limitations of the cavity make only a few reactions possible to observe it under VSC. Some of the reactions are prins cyclisation, deprotection reaction of an alkynylsilane, 1-phenyl-2-trimethylsilylacetylene (PTA) etc.

One of the earlier demonstrations of VSC was the influence of VSC on the ground-state chemical reactivity of deprotection reaction of an alkynylsilane, 1-phenyl-2-trimethylsilylacetylene (PTA), with tetra-*n*-butylammonium fluoride (TBAF). In this experiment, PTA is a pure liquid and injected directly into a microfluidic FP cavity. Here, deprotection reaction follows pseudo-first-order kinetics, and the timescale of reaction is in minutes. 6µm spacer was used inside the optical cavity and tuned cavity precisely to be in resonance with stretching transition of C-Si bond (860cm-1) and along with it $-Si(-Me)_3$ also get coupled. Under Vibrational strong coupling, the reaction rate constant was decreased by a factor of 4.5.[20]

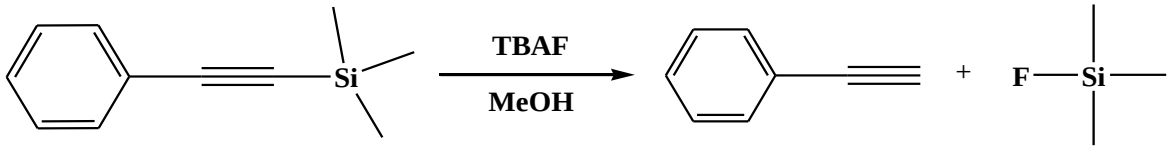

Scheme 1.1: The silane deprotection reaction of 1-phenyl-2-trimethylsilylacetylene.

Recently, K.Hirai and H. Uji-i demonstrated how VSC could affect ketones and aldehydes undergoing Prins-cyclisation reaction. They coupled carbonyl stretching band of various aldehydes and ketones under VSC and observed the decline in the second-order rate constant. They also observed the effect of VSC on thermodynamic parameters like activation energy and enthalpy. The energy of activation was enhanced due to VSC, but the mechanism path of reaction remained the same due to proportional changes in enthalpy of activation.[21]

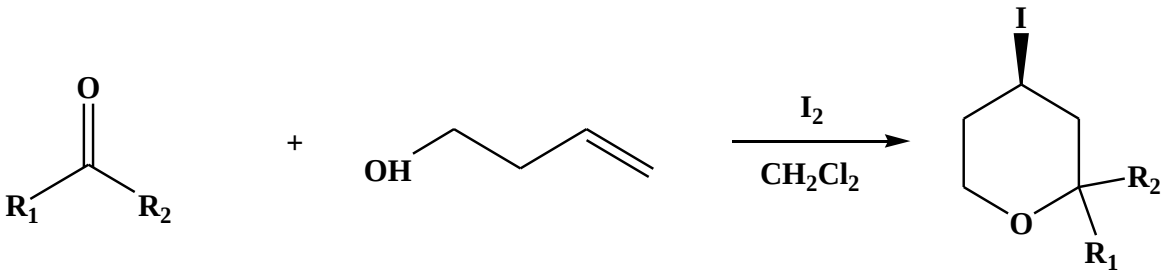

Scheme 1.2: Prins cyclisation reaction in the presence of I_2.

In a different attempt, they showed the evidence of VSC could be used in selective crystallisation. In this experiment, solvent (water) was coupled inside the optical cavity and saw the effects on ZIF MOFs' crystallisation. They observed that two different crystals, ZIF-8 and ZIF-L, were forming in different yields in free solution. However, when -OH stretching vibration was coupled strongly inside the optical cavity, the solution selectively crystallises in ZIF-8 crystals. These experiments elicit the application of VSC in a broader perspective of chemistry.[22]

Recently, our lab at IISER Mohali showed that VSC has potential applications in catalysis and enzymatic reaction by demonstrating the experiment on α chymotrypsin. On selective VSC of O-H stretch of water and O-H and N-H stretching vibrations of the enzyme, the rate of hydrolysis was reported to be changed and catalytic efficiency also enhanced by more than 7 times.[23]

It is evident from the above literature discussion that on changing the chemical bond vibrational energy, the chemical reactions' ground state potential energy surface is also getting perturbed. The major objective of the current project is to study the effects of VSC on solvolysis reactions that involve water as a universal solvent.

Chapter 2: Solvolysis of Benzal Chloride under Vibrational Strong Coupling.

VSC can have significant effect on reaction rate and its mechanism. Reports show, the mechanism change from associative to dissociative, reaction rates showing large changes, enzyme's catalytic efficiency can be boosted and so on.[20] Since the field is growing a general mechanism of how VSC works is not fully understood. In the way of understanding the underlying phenomenon, the solvolysis reaction of Benzal chloride and water is chosen. Industrially, it is used to synthesize benzaldehyde which involves the same hydrolysis reaction.

Here, Co-operative coupling was used to couple the vibrational transition of interest. In this, the solvent is chosen in such a way that it has overlapping vibrational frequency with the solute. In literature [23], a similar experiment is reported in which VSC through co-operative mechanism is used to modify enzyme catalytic efficiency. Enzyme hydrolyses the ester group of para-nitrophenyl acetate (PNPA) and follows the concerted proton transfer process (rate-determining step), leading to a para-nitrophenoxide ion formation. The surrounding water molecules around the enzyme also play a vital role in the catalytic process. OH and NH stretching of alpha-CT and OH stretching of water were coupled through co-operative VSC to see the effect on the reaction mechanism. It was observed that VSC of the OH band of water causing an increase in the reaction rate by affecting the rate-determining step. From the reaction rate, it was evident that the co-operative effect has a significant role in modifying reaction potentials.

The objective of this study is to find out the effects of VSC on solvolysis reaction through co-operativity, and more importantly, to increase the understanding of VSC. In this reaction, the C-Cl cleavage is the rate-determining step, so the possibility of coupling the C-Cl stretching mode was explored. In addition, the reaction rate modifications through co-operative VSC of OH stretching mode of water was also observed.

2.1 Benzal Chloride Solvolysis Reaction.

There is plenty of solvolysis reactions available in the literature. Scheme 2.1 represents solvolysis of benzal chloride reaction. Benzal chloride hydrolyses when dissolves in water and forms benzaldehyde and hydrochloric acid as a by-product. Reaction goes by a Nucleophilic Substitution Unimolecular (S_N1) reaction mechanism, shown in Scheme 2.2. First Step is the formation of the carbocation. In the second step, nucleophile (H_2O) attacks the electropositive carbon atom and replaces chloride ion. In the subsequent step lone pair of the oxygen atom of water again attacks the carbon centre to form benzaldehyde with the formation of HCl as the by-product.

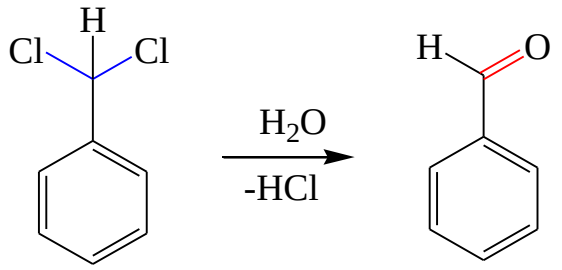

Scheme 2.1: Solvolysis of Benzal chloride in the presence of water.

In literature[24], it is argued that why is the particular mechanism S_N1 is followed. The studies show that the hydrolysis rate of this reaction is independent of the following factors;

- shaking rates
- variation of the ratio of the amount of solution to that of benzal chloride

- pH
- light and oxygen.

While rate is affected a little bit by the addition of nucleophiles, but hydrolysis rate is highly influenced by the chloride ion concentration. The chloride exchange rate in the first step of scheme 2.2 is dependent on the chloride ion concentration, and this step is also slower than the hydrolysis rate. Experiments show that the rate of reaction decreases as the concentration of chloride ions increases.[25]

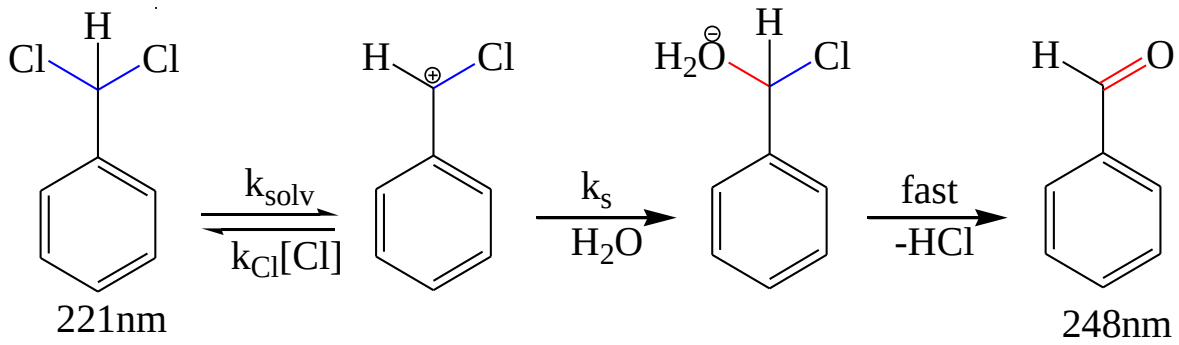

Scheme 2.2: Mechanism of Solvolysis of Benzal chloride in the presence of water.

2.2 Benzal Chloride Solvolysis Reaction mechanisms.

As this reaction goes through the S_N1 mechanism, this section includes why other mechanisms are excluded, and this particular mechanism is selected.

Literature[24,25] showed three mechanisms for hydrolysis of benzal chloride that satisfy the independence of pH and hydrolysis rate and the fact that chloride exchange is slower than that of hydrolysis rate.

Mechanism A

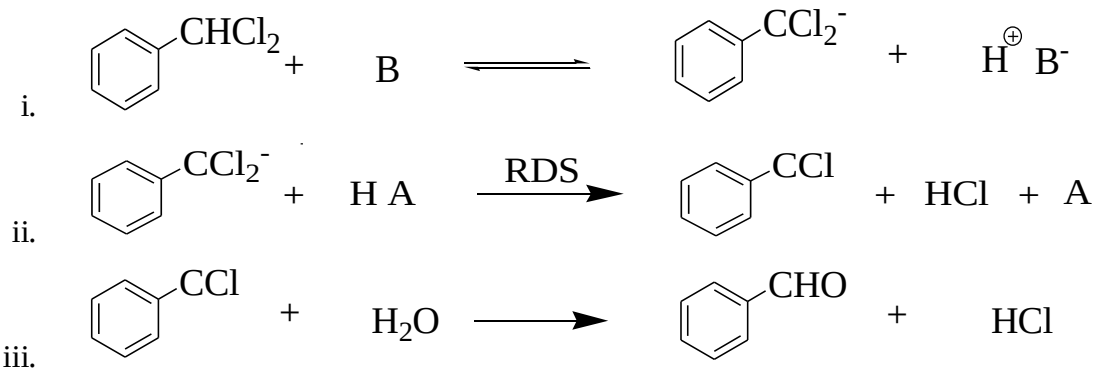

Mechanism B

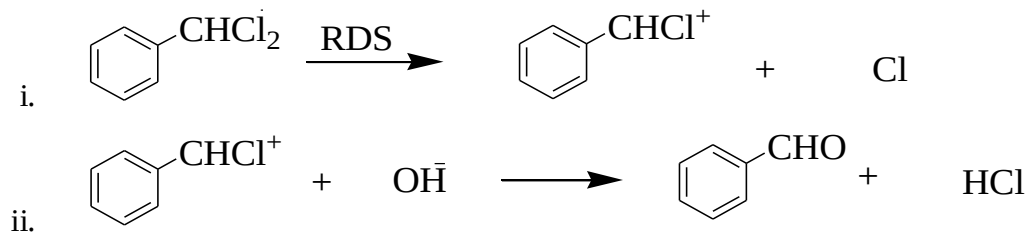

Mechanism C

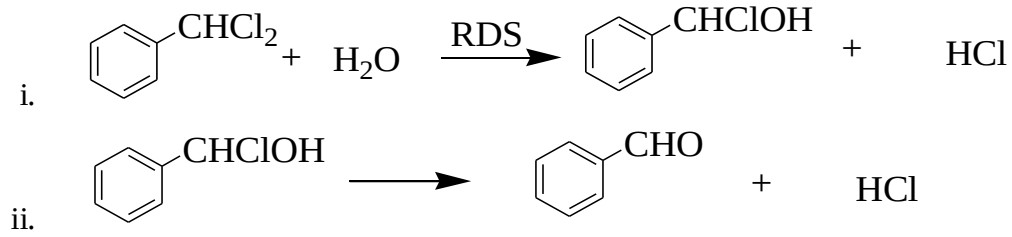

Figure 2.1: Three different possible mechanisms for hydrolysis of Benzal chloride.

In figure 2.1, mechanism A, the rate of hydrogen exchange is faster than the rate of hydrolysis, but experimentally, it was found that it is not the case. In mechanism C, if hydrolysis occurs through bimolecular nucleophilic substitution, then highly nucleophilic

reagents should have accelerated the reaction rate, but experiments show otherwise that the nucleophilic reagents have minimal effect on the rate of reaction. So only mechanism B is the one that is consistent with the experimental results.

Work by B. Colina[26] and the team also showed the consistency of mechanism B in various experiments. They observed the rates of different substituted benzal chloride and found out electron-donating polar substituent (methyl) increases hydrolysis rate while electron-withdrawing polar substituent (chloride) decreases hydrolysis rate as compared to unsubstituted benzal chloride. This rate promoting effect by p-methyl-substituted benzal chloride proves that the electron-deficient centre is present in the transition state and provides strong evidence for the carbocation mechanism. In the studies, it is also showed that hydrolysis is inhibited by dioxane. It follows the rule that less polar solvents inhibit the reaction when the transition state is more polar than the ground state, which is also evidence for mechanism B in figure 2.1.

2.3 Literature analysis of the kinetics of the reaction.

The reaction can be followed by observing the change in absorbance (λ_{max} of either reactant or product) with time. As with time, reactant will convert to product, and so the intensity of absorbance of reactant will decrease, and product will increase with time. The maximum absorbance (λ_{max}) of the reactant, benzal chloride, is 221 nm, and λ_{max} of the product, benzaldehyde, is 248nm. The reaction of 30µL of 0.01M solution of benzal chloride in ACN with 3ml water was initiated. The final concentration of benzal chloride in the reaction remained 0.1mM. The reaction followed pseudo-first-order kinetics. Using the kinetic plots of the reaction value of rate constant was found to be 2.4×10^{-3} s^{-1}.[27]

2.4 IR spectra of Benzal chloride.

Benzal chloride consists of 15 atoms with 39 normal modes of vibrations. The molecular structure of this compound has a C_s point group of symmetry. The reported vibrational assignments of FTIR of this compound are following[28];

- *C-H* vibrations
  - → *Stretching* – 3100 to 3000 cm^{-1}
  - → *In-plane bending*– 1290 to 990 cm^{-1}
  - → *Out-plane bending*– 910–660cm−1
- *C=C* vibrations – 1650 to1430 cm^{-1}
- *C-Cl stretching* vibrations – 730 to 580 cm^{-1}

C-Cl stretch vibrations generally give strong bands.

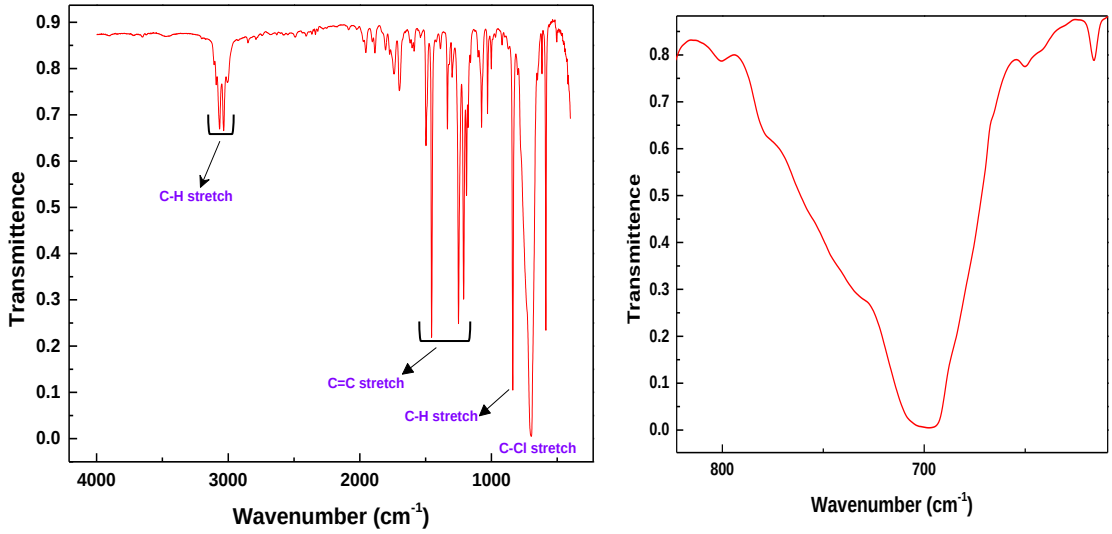

Figure 2.2: FTIR spectra of pure benzal chloride in Non-Cavity and zoomed view of C-Cl stretching band.

The FTIR spectrum of pure benzal chloride with a path length of 6µm was taken and the vibrational frequencies were in good agreement to those reported in the literature. C=C stretch was present around 1400 cm^{-1}. From 3000-3100 $cm^{-1,}$ C-H stretch was present, and C-Cl stretching was found to be the very intense peak, present at 697.5cm^{-1} (figure 2.2).

For examining the rate of a reaction under the cavity, the idea was to couple the strong vibrational mode of the molecule around the reaction centre or the rate-determining step of the reaction under the optical cavity and to see the effect of VSC on the rate of the reaction. Since the RDS was breaking of C-Cl bond, a strong C-Cl stretch was selected to couple under the optical cavity. For doing the hydrolysis, particular concentrations of benzal chloride were prepared in acetonitrile, in which benzal chloride forms a homogenous and transparent solution. In order to determine the shift of C-Cl stretching frequency in ACN, FTIR spectra of 1 M benzal chloride solution with 12µm path length (figure 2.3) was taken. The stretching frequency of the C-Cl bond was found nearly at 706 cm^{-1}.

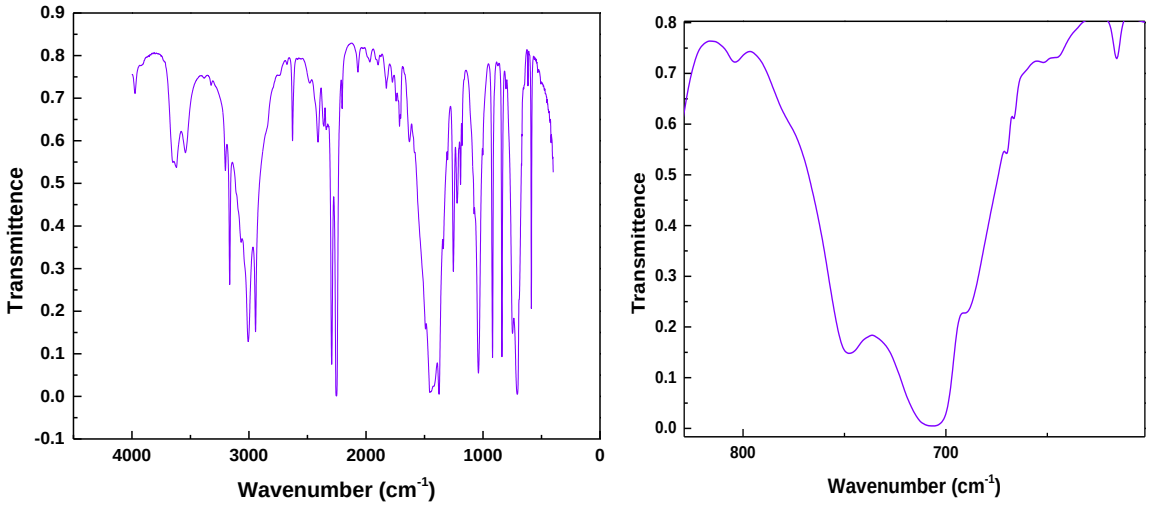

Figure 2.3: FTIR spectra of 1M benzal chloride mixture with ACN in Non-Cavity and zoomed view of C-Cl stretching band.

2.5 Solvolysis reaction of Benzal chloride in a cuvette.

At first, reaction of 0.1mM benzal chloride Solvolysis as reported in section 2.3 was done in a cuvette with a path length of 1cm. Different sets were performed.

Then time-based kinetics program in UV spectrophotometer was used to monitor the progress of reaction after every 5 sec for 30min. The same trend as in literature was observed, with time 220nm peak of reactant decreased and 249nm product peak increased in the UV spectrum (figure 2.4).

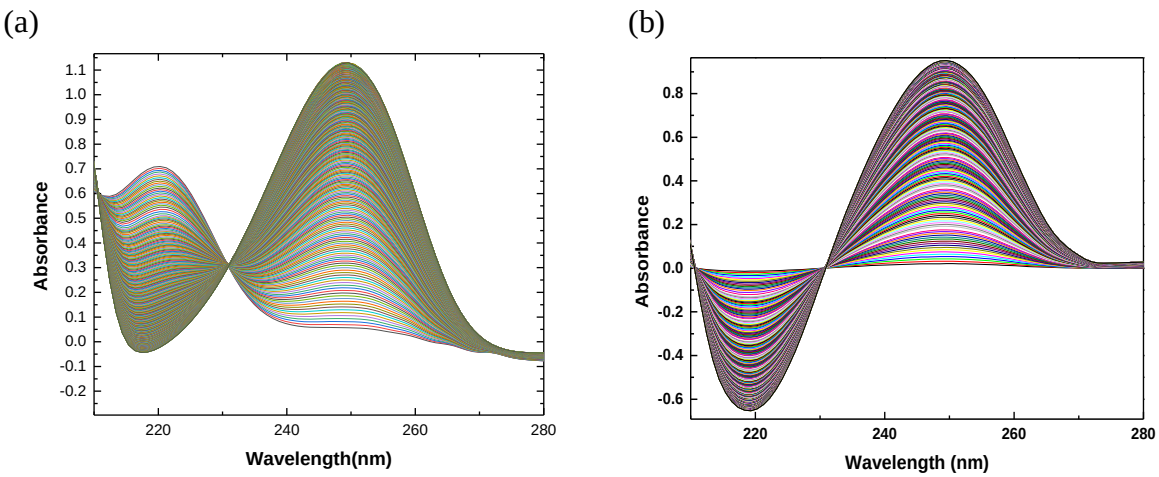

Figure 2.4: Time-based UV-Vis spectrum of solvolysis of 0.1mM benzal chloride in water in cuvette (a) baseline with air and (b) baseline with reaction.

The reaction was monitored at both 249nm and 220nm to measure the observed rate constant. Exponential and linear fit were done. The final rate constant for reaction in cuvette came out to be 2.0 x 10^{-3} sec^{-1}. (figure 2.5).

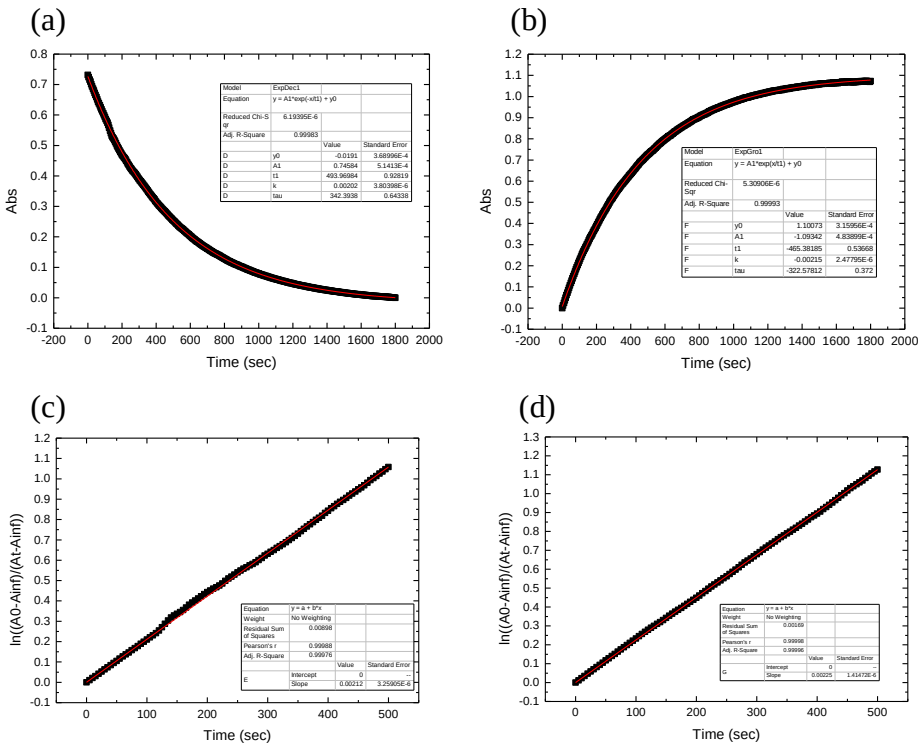

Figure 2.5: (a) Exponential curve for the decay of benzal chloride at 220nm, (b) exponential curve for the formation of benzaldehyde at 249nm, c) linearly fitted kinetic plot for the decay of benzal chloride at 220nm, and d) linearly fitted kinetic plot for the formation of benzaldehyde at 249nm.

2.5.1 Beer-Lambert's Law.

By using concentrations 0.05mM, 0.15mM and 0.2mM Beer-lambert's curve (figure 2.6(b)) was plotted using the absorbances of each concentration at 249nm and plotted against the concentration of the solution. The slope of the curve gave the value of the molar extinction coefficient.

Following is the equation for Beer Lambert's law;

$$A = \varepsilon c l$$

Here, A is absorbance, c is the concentration (in M), l is path length (in cm), and ε is molar extinction coefficient (in M^{-1} cm^{-1}). In curve(b), absorbance is taken on the y-axis, and

concentration is taken on the x-axis. The slope here gives the value of εl, here the value of l is 1cm. So from the curve, the obtained value of ε is ,

$$\varepsilon = 12862.6018 \cong 1.3 \times 10^4\ M^{-1}cm^{-1}$$

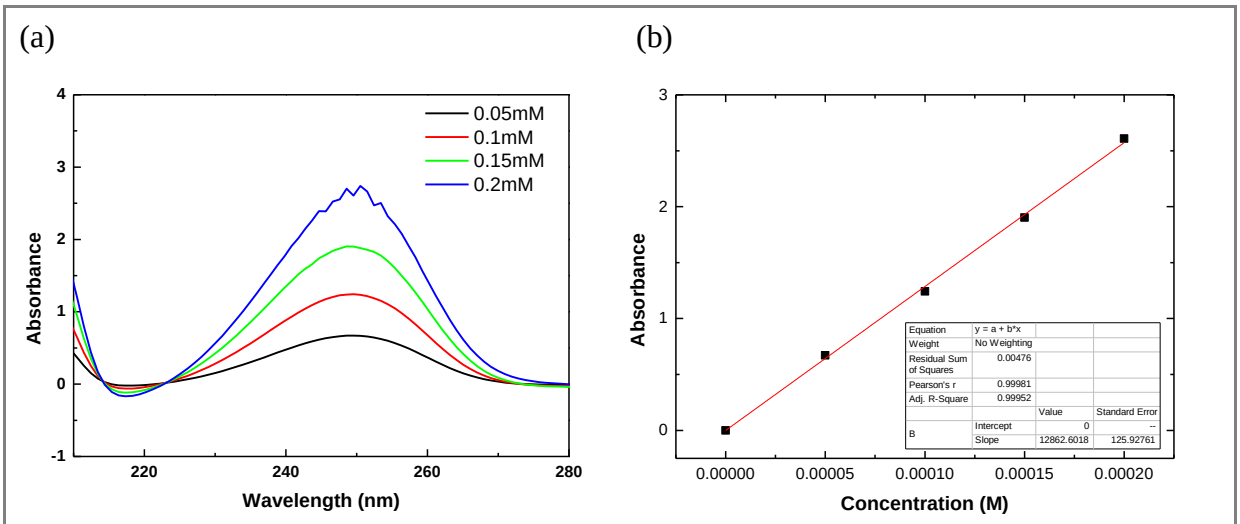

Figure 2.6: (a) Absorption spectra of benzal chloride hydrolysis reaction when the reactant almost converted to product at concentrations of 0.05mM (black), 0.1mM (red) , 0.15mM (green) and 0.2mM (blue). (b) Beer-Lambert's curve; absorbance of each reaction mixture plotted against concentration and the ε value of slope obtained is $3 \times 10^4\ M^{-1}cm^{-1}$.

2.6 Solvolysis reaction of Benzal chloride in Non-Cavity.

In non-cavity conditions, the reaction mixture is injected inside the two barium fluoride substrates with a spacer between them. The path lengths used were 6µm and 12 µm. The path length of non-cavity is much smaller than that of the cuvette. The hydrolysis of benzal chloride was performed with different concentrations of benzal chloride to maintain the condition of pseudo-first-order.

In the cuvette experiment reported above, optical density (OD) of 1 was obtained. Now, as the path length in demountable cell decreased from 1cm to 6µm or 12 µm almost a hundred

times, so in order to get at least OD of 0.1 in cell/cavity, the concentration should also be increased by hundred times.

So in non-cavity conditions, increasing the concentration of benzal chloride in the reaction step by step was tried.

2.6.1 Hydrolysis of 0.9mM Benzal chloride.

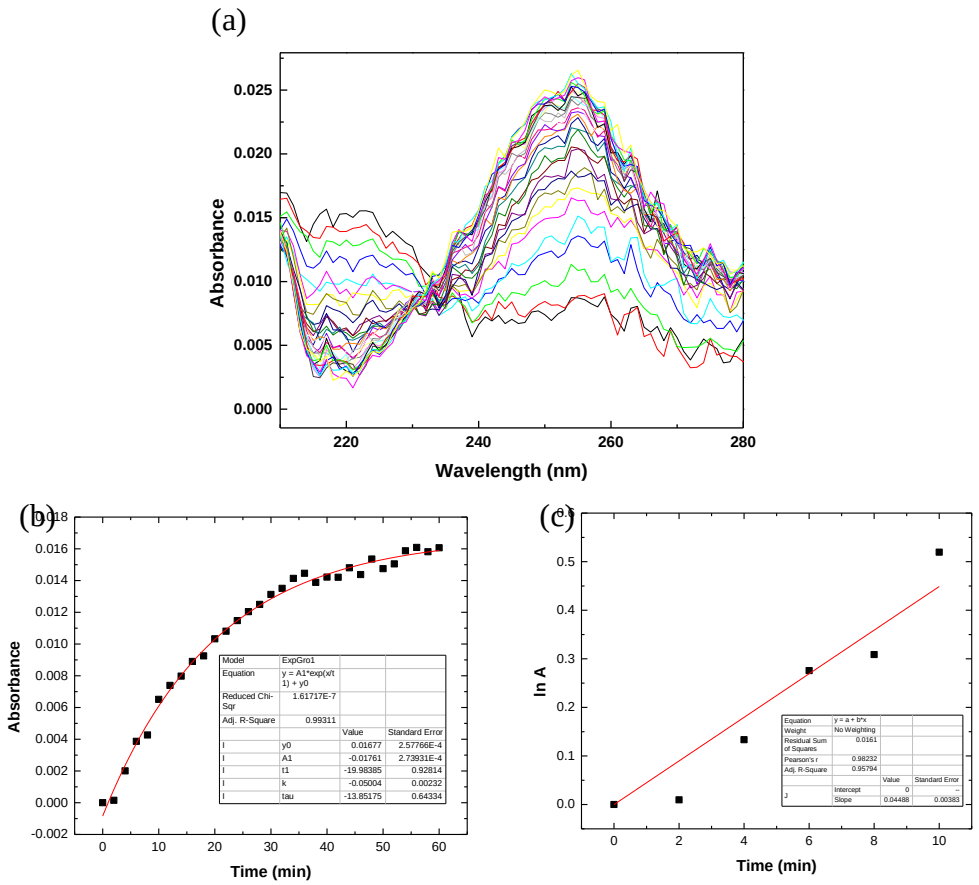

Figure 2.7: (a) Time-based UV-Vis spectrum of 0.9mM benzal chloride in water in non-cavity conditions. (b) exponentially fitted and (c) linearly fitted kinetic plots of product formation in the reaction in Non-cavity conditions at 249nm.

Firstly, the concentration of the benzal chloride in the solution was increased by nine times. For this, 100µl of 0.01M Benzal Chloride solution diluted in ACN was taken and added 1000µl of water. The reaction mixture was homogenous. The final concentration of benzal chloride in the solution became 0.9mM. This reaction mixture was immediately injected into the demountable cell using a syringe. Time-based kinetics program in UV spectrophotometer was used to monitor the progress of reaction every 2 min for 1 hr., which gave the following spectra in figure 2.7 (a). The reaction was monitored at 248nm, which represents the formation of the product, to measure the observed rate constant in this pseudo-first-order reaction. Exponential and linear fit both were done, and the final rate constant for reaction in non-cavity obtained was 8.3 $x10^{-4}$ sec^{-1}, shown in figure 2.7(b) and (c), respectively.

In this case, the maximum OD of the reaction recorded was around 0.03, so to increase the OD value, concentration of benzal chloride in the solution was further increased.

2.6.2 Hydrolysis of 10mM Benzal chloride.

For keeping the final concentration of benzal chloride 10mM, 60µl of 0.1M benzal chloride (in ACN) was added to 540µl water. And as mentioned above, the kinetics of this reaction was observed by UV-spectrophotometry at 249nm, shown in figure 2.8. The observed rate constant of the reaction was 1.8 $x10^{-4}$ sec^{-1}.

But the reaction mixture, in this case, was turbid, not mixed homogenously in the solution. So in order to enhance solubility by keeping the final concentration same (10mM), the amount of solvent- ACN in the mixture was increased by adding 120µl of 0.05M Benzal Chloride (in ACN) in 480µl water. As a result, the amount of water for this reaction decreased. But the solution here also was showing a little bit of turbidity. The progress of the reaction was recorded after every 5 seconds for 20 minutes. The spectrum of the following reaction and exponential plot for the 249nm is shown in figure 2.9. In this reaction, the observed rate constant was 1.1 $x10^{-3}$ sec^{-1}, ten orders higher than the above reaction of 10mM benzal chloride. The possible reason behind this scenario can be the turbidity of the solution,

and the reactant was not mixing homogenously in the solution. The OD, in this case, also was going up to 0.03 only.

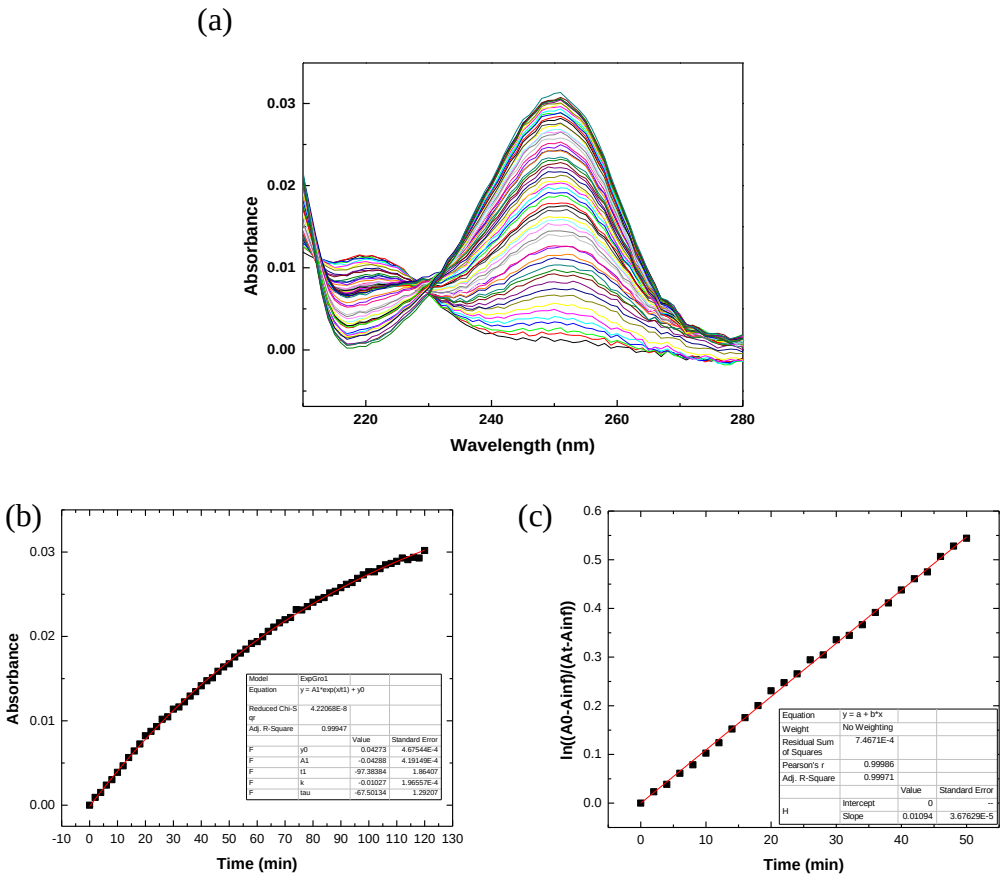

Figure 2.8: (a) Time-based UV-Vis spectrum 10mM of benzal chloride in water in non-cavity conditions. (b) exponentially fitted and (c) linearly fitted kinetic plots of product formation in the reaction in Non-cavity conditions at 249nm.

2.6.3 Hydrolysis of 5mM Benzal chloride.

In the above case of the 10mM hydrolysis reaction, both the reaction mixture was turbid. So in order to increase solubility, the final concentration of benzal chloride in the solution was decreased such that OD does not decrease much.

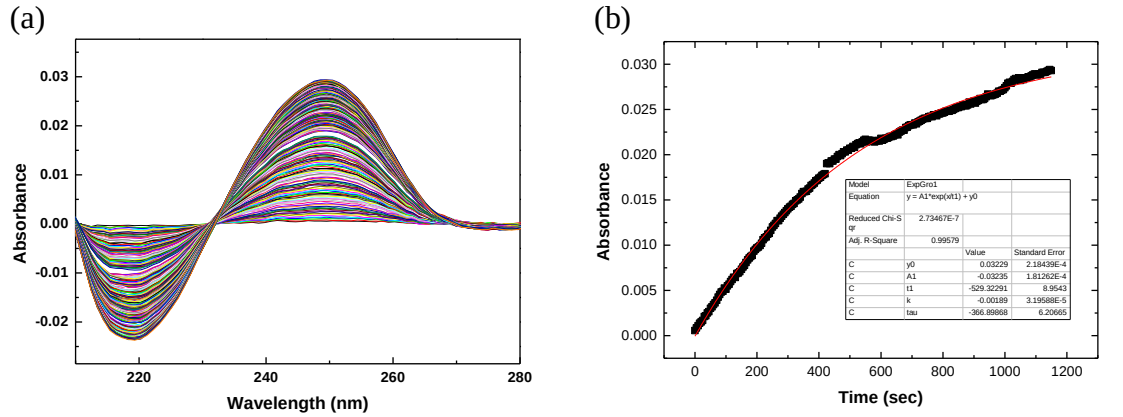

Figure 2.9: (a) Time-based UV-Vis spectrum of 10mM benzal chloride in water in non-cavity conditions. (b) exponentially fitted kinetic plot of formation of product in the reaction in Non-cavity conditions at 249nm.

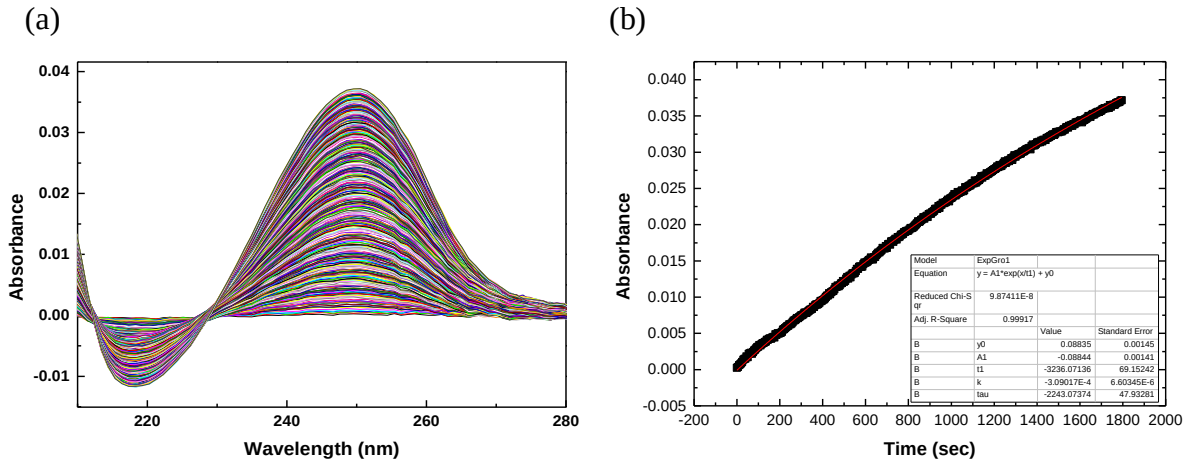

Figure 2.10: (a) Time-based UV-Vis spectrum of 5mM benzal chloride in water in non-cavity conditions. (b) exponentially fitted kinetic plot of formation of product in the reaction in Non-cavity conditions at 249nm.

In this case, 30µl of 0.1M benzal chloride (in ACN) was added to 570µl water, and the final concentration of reactant becomes 5mM in the solution. The reaction mixture formed was a little bit turbid, but after few seconds, it became homogenous. Using the similar technique mentioned above, the kinetics of this reaction was observed at 249nm (figure 2.10). The rate constant observed for this reaction was very less, around 3.0 $x10^{-4}$ sec^{-1}.

2.7 Solvolysis reaction of Benzal chloride in cavity.

In the previous chapter, it is already discussed about the setup and working of the FP-cavity. The actual picture of an FP-cavity is shown in figure 2.11. The main goal in this current study is to understand the effect of VSC in modifying the chemical rate of the reaction. Here, VSC of C-Cl stretch of benzal chloride (~700cm^{-1}), which is directly involved in the rate-determining step is tried.

(a) (b)

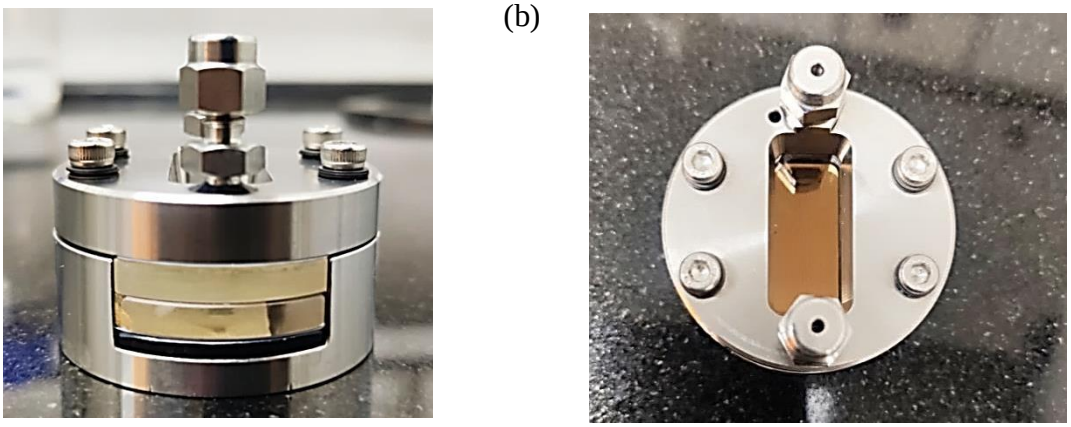

Figure 2.11: Picture of the FP cavity (a) lateral view and (b) top view of cavity.

But by using BaF_2 substrates, which are not IR transparent below 800cm^{-1}, so it was very difficult to observe whether the coupling was happening or not. So to observe co-operative effects in the kinetics of the reaction by attack of water on the reaction centre by VSC of O-H stretching band (~3600-3200cm^{-1}) was done, as water also plays a major role in this reaction. The FTIR spectrum of water is shown in figure 2.12.

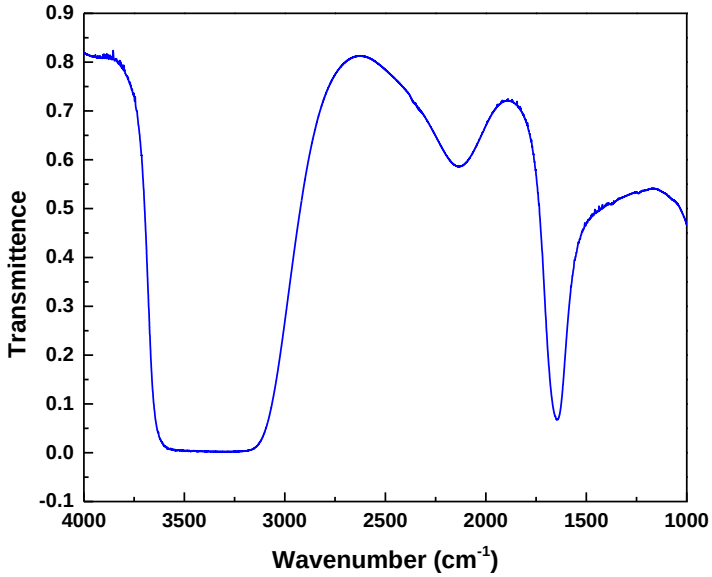

Figure 2.12: FTIR spectra of Water in Non-Cavity condition with 6µm spacer.

2.7.1 Hydrolysis of 0.9mM Benzal chloride.

The same reaction mentioned in section 2.6.1 done in non-cavity condition was repeated in cavity conditions. Firstly cavity with 12µm was tuned precisely to couple with C-Cl stretching frequency (figure.2.13). The FSR of the empty cavity was 312.39 cm^{-1}. After injecting the reaction mixture in the cavity refractive index changed from 1 (air) to 1.34 (reaction mixture), due to which the FSR of the cavity changed to 231.71 $cm^{-1,}$ and the third mode of the cavity was approximately 695.13 cm^{-1} which was nearly similar to the C-Cl stretching frequency.

Then time-based UV spectrum was recorded, shown in figure.2.14(a). The reaction was monitored at 249nm and measured the apparent rate constant in cavity conditions. The final rate constant for the reaction in the cavity obtained was 1.1 $x10^{-3}$ sec^{-1}, shown in figure 2.14 (b) and (c), respectively.

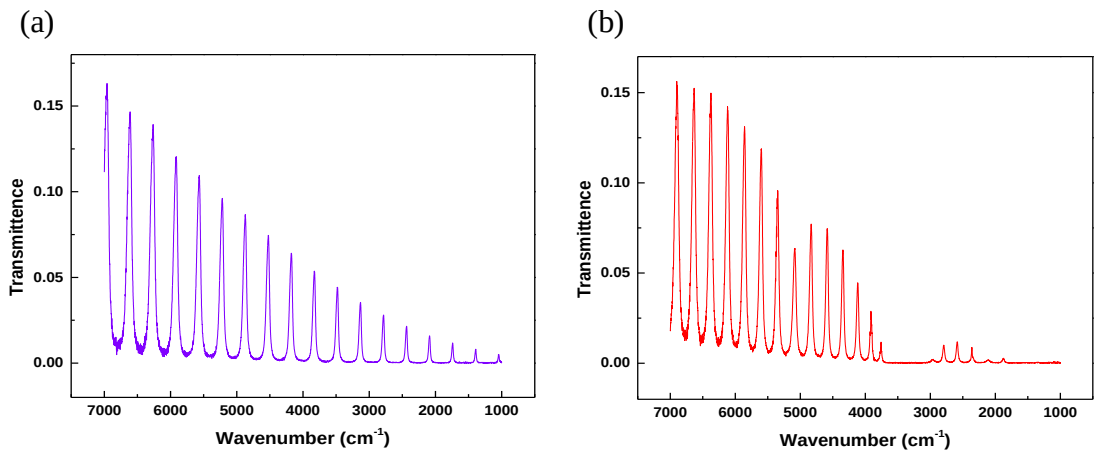

Figure 2.13: Optical modes of the cavity (a) before injection (empty cavity) and (b) after injection (on resonance cavity).

Only a little bit of change of observed rate constant was found in cavity conditions compared to non-cavity condition. But in this case, because of the low transparency of BaF_2 below 800 cm^{-1}, it was not sure whether the coupling of C-Cl stretch was happening strongly or not. So for the next reaction, the VSC of the O-H stretch of water was done to observe cooperative mechanism.

2.7.2 Hydrolysis of 10mM Benzal chloride.

For 10mM concentration of benzal chloride in solution, the reaction of 120µl of 0.05M Benzal Chloride (in ACN) was added to 480µl of water. In this reaction, coupling of the O-H stretch of water was tried. For this, 6µm spacer was used, as in 12µm spacer, it will be very difficult to do an off-resonance experiment for this reaction. For this microfluidic cavity was precisely tuned to vibrationally couple with O-H stretch of water such that FSR after injecting the reaction mixture became 477.23cm^{-1} and seventh mode of the cavity (3340.561cm^{-1}) came in resonance with O-H stretch. In another case, the cavity was set in such a way that after injection, cavity mode is off-resonance with O-H stretch of water. The FSR in this case after injecting the reaction mixture was 462.52$cm^{-1,}$ and the seventh and eighth mode of the cavity was 3237.654cm^{-1} and 3700.176 $cm^{-1,}$ respectively. But in both

cases, rabi splitting was observed, and VSC is happening in both cases due to a very broad band of O-H stretch. The FTIR spectra of both cases are shown in figure.2.15.

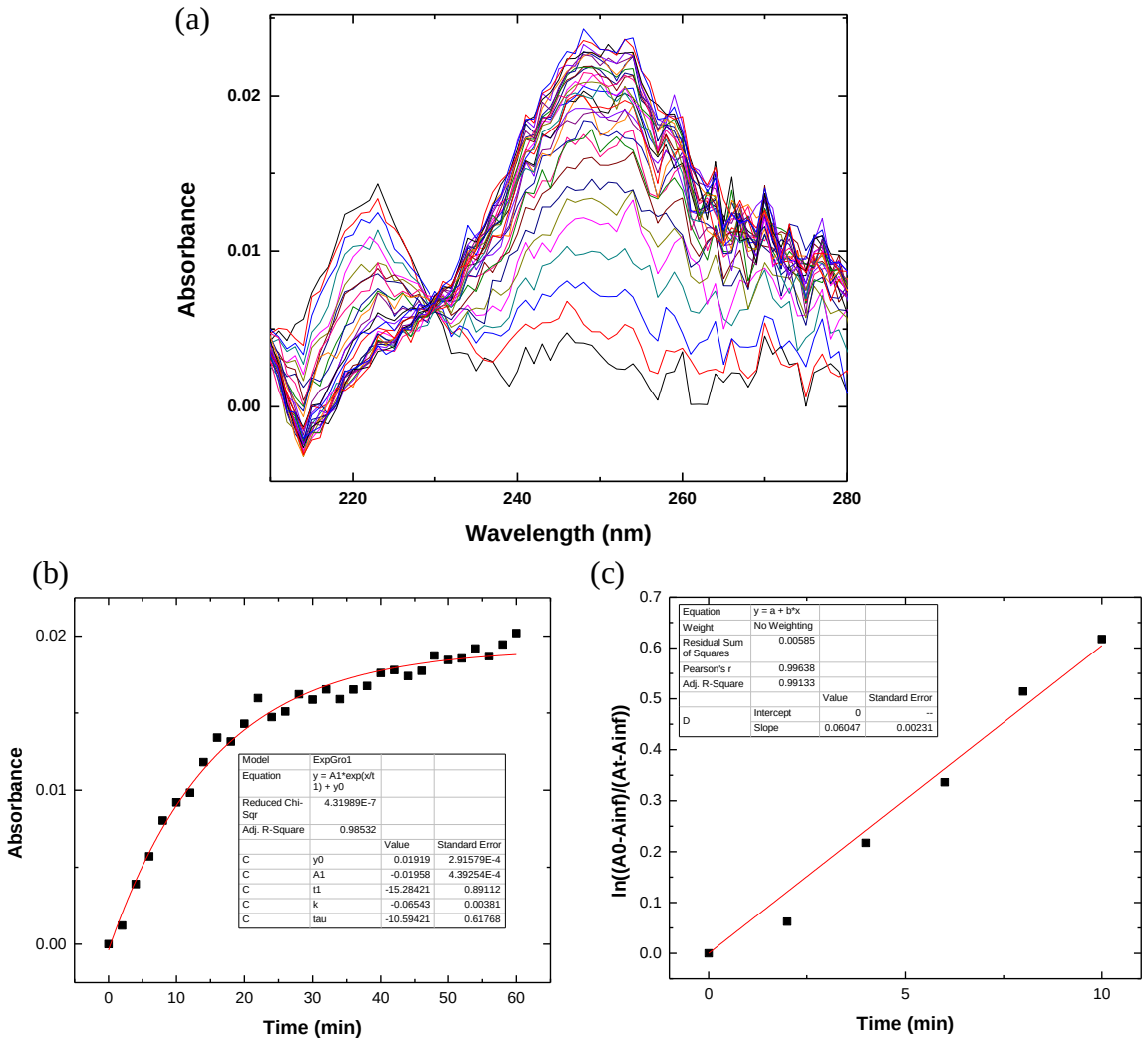

Figure 2.14: (a) Time based UV-Vis spectrum of 0.9mM benzal chloride in water in cavity conditions. (b) exponentially fitted and (c) linearly fitted kinetic plots of formation of product in the reaction in cavity conditions at 249nm.

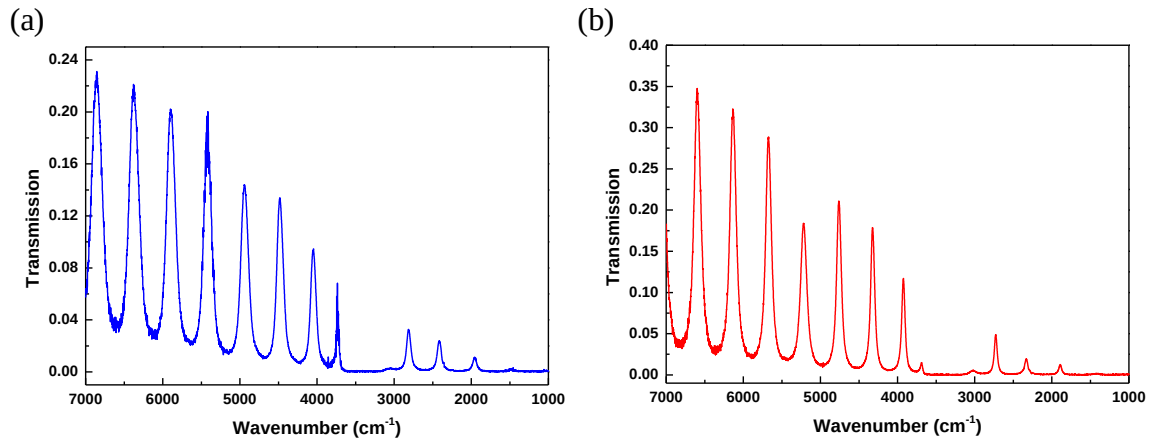

Figure 2.15: Optical modes of the cavity (a) on-resonance with O-H stretch and (b) off-resonance with O-H stretch.

Then time-based kinetics of both the cases were recorded using spectrophotometry, shown in figure 2.16. The reaction was monitored at 249nm, but the kinetic plots were very irregular and deviating from the exponential curve; because of this, determination the rate of the reactions in the cavity was not possible.

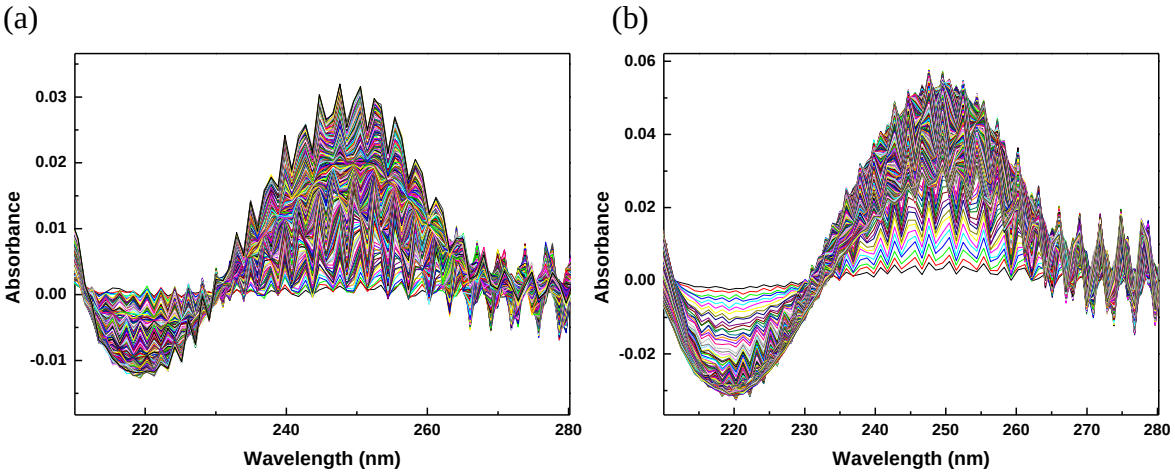

Figure 2.16: Time based UV-Vis spectrum of 10mM benzal chloride in water in cavity conditions. (a) On-resonance with O-H stretch and (b) Off-resonance with O-H stretch.

S.No	Benzal chloride concentration	Reaction with	Condition	Rate constant (sec^{-1})
1	0.1mM	H_2O	Cuvette	2.0×10^{-3}
2	0.9mM	H_2O	Non-cavity	8.3×10^{-4}
3	10mM	H_2O	Non-cavity	1.8×10^{-4}
4	10mM	H_2O	Non-cavity	1.1×10^{-3}
5	5mM	H_2O	Non-cavity	3.0×10^{-4}
6	0.9mM	H_2O	Cavity	1.1×10^{-3}
7	10mM	H_2O	Cavity	Not determined

Table1- Summary of experimental data with their rate constants.

In the above rate constant, there was very much inconsistency. Even for the same concentration, the difference in rate was ten times varying. It was not even consistent with the increase or decrease of concentration in a non- cavity. For cavity, the reaction was very difficult to observe. There can be various possible reasons for this which are stated in the next section.

2.8 Results and Discussion.

2.8.1 Possible factors for deviation of the reaction from pseudo-first-order.

- The concentration of Benzal Chloride in 0.9mM hydrolysis reaction is very less, causing difficulty in getting enough coupling strength. And also, coupling strength in this with C-Cl stretch could not be detected due to the opaqueness of BaF_2 substrate below $800cm^{-1}$.

- The solubility of benzal chloride is very low in water which limits us to go higher in concentration. On a higher concentration of benzal chloride, the solution is turbid and does not mix homogeneously in water which can be one of the reasons that the reaction does not follow exponential growth (pseudo-first-order).
- As to reach up to OD of 0.1 in the cell, the concentration of solution should be increased 100 times, i.e. 10mM, which leads to more production of HCl, and the reaction mixture turns more acidic. It can be another reason hindering the reaction by changing the pH of the reaction or by shifting the equilibrium towards the reactant. As per literature [24], hydrolysis rate is independent of the pH, so accordingly, the pH factor can be eliminated. And the most significant reason is more chloride production in the solution, which is hindering the reaction and slowing down the rate.
- Here in the cell/ cavity, the amount of water is decreasing compared to the cuvette, and the path length of the cell is very small, due to which mobility of molecules becomes difficult due to congestion.

In order to solve these problems, firstly, the pH of the different reaction mixture was measured. By using the pH value, the concentration of chloride ions was calculated and using that concentration; base catalysed reaction was thought to be done so that the base can remove the HCl by-product and hence catalysed the reaction. This procedure results in the shifting of equilibrium towards the product. The second possible solution is to do the same reaction in buffer solution, as the buffer will consume the HCl by-product and also hamper the change in pH (which was assumed that pH is not causing the change of reaction pathway).

2.8.2 pH measurements.

20ml reaction mixtures of four different concentrations (0.1mM, 0.5mM, 2mM and 5mM) of benzal chloride were prepared using stock solution of 10mM and 100mM. Before every measurement, the pH meter was calibrated using buffer solutions of pH 7 and 4, respectively.

The pH of water used in the reaction was nearly 7. Then different concentration and volume of benzal chloride were added to prepare the desired reaction mixtures and measured the pH until the reaction got finished.

The observed pHs of the mixtures are reported below in table 2. As the concentration of benzal chloride in the reaction mixtures was increasing, the amount of HCl produced also increased, and solutions were becoming more acidic.

S.No	Benzal chloride concentration in water	pH
1.	0.1mM	3.45
2.	0.5mM	2.96
3.	2mM	2.64
4.	5mM	2.4

Table 2- pH of solutions with different concentration of benzal chloride

2.8.3 Base catalysed reaction.

For 2mM benzal chloride hydrolysis, the concentration of chloride ion in the product was calculated using pH, which came around 2.3mM. Then NaOH aqueous solution of the same concentration of 2.3mM was prepared such that all the chloride ions in the solution get consumed by sodium ions, and the chloride ion cannot hinder the forward reaction.

Reaction of 2mM benzal chloride was done with 2.3mM aqueous NaOH solution in the microfluidic cell and measured the kinetics using a spectrophotometer for 1hr in 10sec interval. UV spectra and kinetic plots of the reaction are shown in figure 2.17. The rate constant observed for this reaction was around 1.1×10^{-3} sec^{-1}.

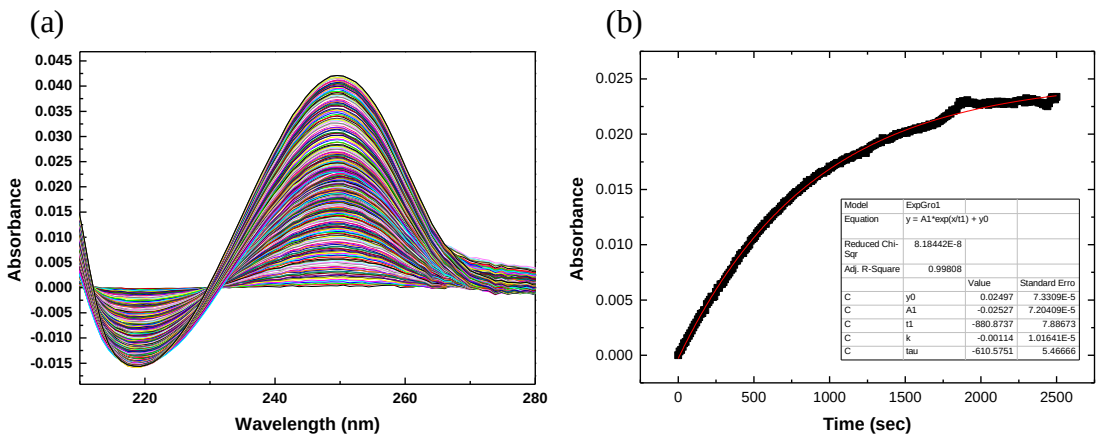

Figure 2.17: (a) Time-based UV-Vis spectrum of 2mM benzal chloride in aqueous in non-cavity conditions. (b) exponentially fitted kinetic plot of formation of product in the reaction in cavity conditions at 249nm.

2.8.4 Hydrolysis Reaction in Buffer solution.

For performing benzal chloride hydrolysis, a Trizma buffer of neutral pH was chosen.

A. Preparation of Trizma buffer.

For preparation of 0.05M Tris buffer of neutral pH of 7.2, the standard guidelines were followed. For 10ml of required buffer solution, 70.2mg of Trizma-HCl and 0.67mg of Trizma-Base were added in 10 ml of water and stirred the mixture till both acid and base solubilise in water.

B. Hydrolysis of 5mM Benzal chloride.

30µl of 0.1M benzal chloride solution (in ACN) was added to 570µl of Trizma buffer solution such that the final concentration of benzal chloride remains 5mM in the reaction mixture. The reaction was performed in non-cavity conditions. The reaction was kept for 1hr inside the spectrophotometer, and UV spectra were recorded every 10sec, shown in figure

2.18 (a). Kinetics of the reaction for pseudo-first-order for 249nm observed (2.18(b)). The observed rate constant for this reaction was 8.5 x10^{-4} sec^{-1}.

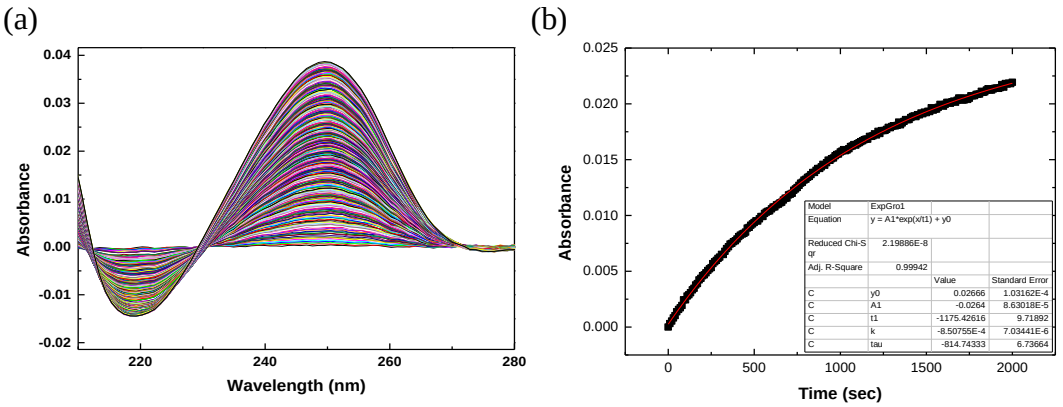

Figure 2.18: (a) Time based UV-Vis spectrum of 5mM benzal chloride in buffer solution in non-cavity conditions. (b) exponentially fitted kinetic plot of formation of product in the reaction in cavity conditions at 249nm.

2.9 Conclusions.

Solvolysis reaction of benzal chloride with water follows nucleophilic substitution unimolecular (S_N1) reaction mechanism. Here, the first step (i.e. formation of carbocation) is the rate-determining step. We thought of coupling the C-Cl bond to the vacuum field, which was a freshers perspective. The C-Cl stretching frequency is around 700cm^{-1}. The technical limitation and the weak oscillator strength of the C-Cl limit us from doing further experiments in the regime. In the next step, we tried the coupling of –OH stretching because the H_2O attacks the carbocation and involved in the solvolysis process.

We found that the reaction is behaving perfectly in the cuvette (1cm path length). But when it comes to microfluidics cell, which is of significantly smaller path length (~10 um) than the cuvette, the solution has homogeneity issues that trigger diffusion limited kinetics. Additionally, we need to ramp up the concentrations to very high levels (nearly 100 times than normal) to obtain the readable optical density, which is also crucial in the kinetics measurements. Here, benzal chloride is sparingly soluble in water and prohibits us from going to high concentrations to probe the reaction kinetics in the UV-VIS regime. Despite the problems mentioned above, we firmly believe that this problem can be worked out but requires much more extensive optimisations. We also put forward other solutions to the problem by choosing a solvent better than water. Further studies can be continued using different reactant concentrations with base-catalysed and buffer mediated reactions.

••••

Bibliography

(1) Atkins, P.; Overton, T. *Shriver and Atkins' Inorganic Chemistry*; Oxford University Press, USA, 2010.

(2) Simpson, W. T.; Peterson, D. L. Coupling Strength for Resonance Force Transfer of Electronic Energy in Van Der Waals Solids. *The Journal of Chemical Physics*. 1957, pp 588–593. https://doi.org/10.1063/1.1743351.

(3) Kobayashi, T. *J-Aggregates*; World Scientific, 2012; Vol. 2.

(4) Ebbesen, T. W. Hybrid Light–Matter States in a Molecular and Material Science Perspective. *Acc. Chem. Res.* **2016**, *49* (11), 2403–2412.

(5) Purcell, E. M.; Torrey, H. C.; Pound, R. V. Resonance Absorption by Nuclear Magnetic Moments in a Solid. *Phys. Rev.* **1946**, *69* (1–2), 37.

(6) Pockrand, I.; Brillante, A.; Möbius, D. Exciton–Surface Plasmon Coupling: An Experimental Investigation. *J. Chem. Phys.* **1982**, *77* (12), 6289–6295.

(7) Hertzog, M.; Wang, M.; Mony, J.; Börjesson, K. Strong Light–Matter Interactions: A New Direction within Chemistry. *Chem. Soc. Rev.* **2019**, *48* (3), 937–961.

(8) Kolaric, B.; Maes, B.; Clays, K.; Durt, T.; Caudano, Y. Strong Light–Matter Coupling as a New Tool for Molecular and Material Engineering: Quantum Approach. *Adv. Quantum Technol.* **2018**, *1* (3), 1800001. https://doi.org/https://doi.org/10.1002/qute.201800001.

(9) Hertzog, M.; Rudquist, P.; Hutchison, J. A.; George, J.; Ebbesen, T. W.; Börjesson, K. Voltage-controlled Switching of Strong Light–Matter Interactions Using Liquid Crystals. *Chemistry* **2017**, *23* (72), 18166.

(10) Gao, W.; Li, X.; Bamba, M.; Kono, J. Continuous Transition between Weak and Ultrastrong Coupling through Exceptional Points in Carbon Nanotube Microcavity Exciton–Polaritons. *Nat. Photonics* **2018**, *12* (6), 362–367.

(11) Bransden, B. H.; Joachain, C. J. *Physics of Atoms and Molecules*; Pearson Education India, 2003.

(12) Jaynes, E. T.; Cummings, F. W. Comparison of Quantum and Semiclassical Radiation Theories with Application to the Beam Maser. *Proc. IEEE* **1963**, *51* (1), 89–109.

(13) Hopfield, J. J. Theory of the Contribution of Excitons to the Complex Dielectric Constant of Crystals. *Phys. Rev.* **1958**, *112* (5), 1555.

(14) Khitrova, G.; Gibbs, H. M.; Kira, M.; Koch, S. W.; Scherer, A. Vacuum Rabi Splitting in Semiconductors. *Nat. Phys.* **2006**, *2* (2), 81–90.

(15) Agranovich, V. M.; Gartstein, Y. N.; Litinskaya, M. Hybrid Resonant Organic–Inorganic Nanostructures for Optoelectronic Applications. *Chem. Rev.* **2011**, *111* (9), 5179–5214.

(16) Carusotto, I.; Ciuti, C. Quantum Fluids of Light. *Rev. Mod. Phys.* **2013**, *85* (1), 299.

(17) Houdré, R.; Stanley, R. P.; Ilegems, M. Vacuum-Field Rabi Splitting in the Presence of Inhomogeneous Broadening: Resolution of a Homogeneous Linewidth in an Inhomogeneously Broadened System. *Phys. Rev. A* **1996**, *53* (4), 2711–2715. https://doi.org/10.1103/PhysRevA.53.2711.

(18) Hoffmann, R. How Chemistry and Physics Meet in the Solid State. *Angew. Chemie Int. Ed. English* **1987**, *26* (9), 846–878.

(19) Vahala, K. J. Optical Microcavities. *Nature* **2003**, *424* (6950), 839–846.

(20) Thomas, A.; George, J.; Shalabney, A.; Dryzhakov, M.; Varma, S. J.; Moran, J.; Chervy, T.; Zhong, X.; Devaux, E.; Genet, C. Ground-State Chemical Reactivity under Vibrational Coupling to the Vacuum Electromagnetic Field. *Angew. Chemie* **2016**, *128* (38), 11634–11638.

(21) Hirai, K.; Takeda, R.; Hutchison, J. A.; Uji-i, H. Modulation of Prins Cyclization by Vibrational Strong Coupling. *Angew. Chemie Int. Ed.* **2020**, *59* (13), 5332–5335. https://doi.org/https://doi.org/10.1002/anie.201915632.

(22) Hirai, K.; Ishikawa, H.; HUTCHISON, J.; Uji-i, H. Selective Crystallization via Vibrational Strong Coupling. **2020**.

(23) Lather, J.; George, J. Improving Enzyme Catalytic Efficiency by Co-Operative Vibrational Strong Coupling of Water. *J. Phys. Chem. Lett.* **2021**, *12* (1), 379–384. https://doi.org/10.1021/acs.jpclett.0c03003.

(24) TANABE, K.; IDO, T. THE MECHANISM OF THE HYDROLYSIS OF BENZAL CHLORIDE. *J. Res. Inst. Catal. HOKKAIDO Univ. 12* (3), 223–229.

(25) IDO, T.; TANABE, K. THE EXCHANGE REACTIONS OF CHLORINE AND HYDROGEN BETWEEN BENZAL CHLORIDE AND AQUEOUS CHLORIDE SOLUTION. *J. Res. Inst. Catal. HOKKAIDO Univ. 12* (3), 212–222.

(26) Colina, B.; Rotaeche, M. G.; Guerrero, E.; Malpica, A.; Calzadilla, M.; Baumrucker, J. Kinetics and Mechanism for Hydrolysis of Substituted. Alpha.,. Alpha.-Dichlorotoluenes. *J. Org. Chem.* **1974**, *39* (26), 3918–3920.

(27) Jagannadham, V. F. **2006**, No. August, 86–89.

(28) Nagabalasubramanian, P. B.; Periandy, S.; Mohan, S.; Govindarajan, M. FTIR and FT Raman Spectra, Vibrational Assignments, Ab Initio, DFT and Normal Coordinate Analysis of α, α Dichlorotoluene. *Spectrochim. Acta Part A Mol. Biomol. Spectrosc.* **2009**, *73* (2), 277–280.